NMR Conformational Study of the Sixth Transmembrane Segment of Sarcoplasmic Reticulum Ca^{2+}-ATPase†

Stéphanie Soulié,‡ Jean-Michel Neumann,‡ Catherine Berthomieu,§ Jesper V. Møller,|| Marc le Maire,*,‡ and Vincent Forge‡,⊥

Section de Biophysique des Protéines et des Membranes and Section de Bioénergétique, Département de Biologie Cellulaire et Moléculaire, CEA et CNRS Unité de Recherche Associée 2096, CEA Saclay, 91191 Gif-sur-Yvette, Cedex, France and Danish Biomembrane Research Centre, Department of Biophysics, University of Aarhus, DK-8000 Aarhus C, Denmark

Received December 23, 1998; Revised Manuscript Received March 4, 1999

ABSTRACT: In current topological models, the sarcoplasmic reticulum Ca^{2+}-ATPase contains 10 putative transmembrane spans (M1−M10), with spans M4/M5/M6 and probably M8 participating in the formation of the membranous calcium-binding sites. We describe here the conformational properties of a synthetic peptide fragment (E785−N810) encompassing the sixth transmembrane span (M6) of Ca^{2+}-ATPase. Peptide M6 includes three residues (N796, T799, and D800) out of the six membranous residues critically involved in the ATPase calcium-binding sites. 2D-NMR experiments were performed on the M6 peptide selectively labeled with ^{15}N and solubilized in dodecylphosphocholine micelles to mimic a membrane-like environment. Under these conditions, M6 adopts a helical structure in its N-terminal part, between residues I788 and T799, while its C-terminal part (G801−N810) remains disordered. Addition of 20% trifluoroethanol stabilizes the α-helical N-terminal segment of the peptide, and reveals the propensity of the C-terminal segment (G801−L807) to form also a helix. This second helix is located at the interface or in the aqueous environment outside the micelles, while the N-terminal helix is buried in the hydrophobic core of the micelles. Furthermore, the two helical segments of M6 are linked by a flexible hinge region containing residues T799 and D800. These conformational features may be related to the transient formation of a Schellman motif (L_{797}VTDGL_{802}) encoded in the M6 sequence, which probably acts as a C-cap of the N-terminal helix and induces a bend with respect to the helix axis. We propose a model illustrating two conformations of M6 and its insertion in the membrane. The presence of a flexible region within M6 would greatly facilitate concomitant participation of all three residues (N796, T799, and D800) believed to be involved in calcium complexation.

Sarcoplasmic reticulum Ca^{2+}-ATPase belongs to the family of P-type cation-transporting ATPases (see ref *1* for a review). These proteins are characterized by the formation of a phosphorylated intermediate (*E*P) during the catalytic cycle. Basically, the reaction cycle can be formulated in terms of a four step scheme: $E_1 \rightarrow E_1P \rightarrow E_2P \rightarrow E_2 \rightarrow E_1$, with E_1 and E_2 being the two major conformational states (e.g., refs *2*−*10*). Ca^{2+}-ATPase pumps two calcium ions per one hydrolyzed ATP from the cytoplasm into the lumen, leading to the muscle relaxation (*11*).

The exact topology of the Ca^{2+}-ATPase is still a matter of debate, although there is general agreement on the existence of 10 transmembrane (TM)[1] spans (named M1−M10) initially predicted from the amino acid sequence (*12*) and subsequently supported by proteolysis and immunological experiments (reviewed in ref *13*). In the 10-spans model (see Figure 1A), the N-terminal domain comprises TM spans M1−M4, while the C-terminal domain is composed of spans M5−M10. However, plasticity in the insertion of the M7/M8 region has also been shown (*13*). So far there is no high-resolution structure of any P-type ATPase, but tertiary structures at 8 Å resolution of the H^+-ATPase (*14*) and the Ca^{2+}-ATPase (*15*) have been deduced from electron microscopy with 2D ordered specimens and diffraction measure-

† S.S. is the recipient of a fellowship from the Ministère de la Recherche et de l'Enseignement Supérieur and has additional support from the Fondation pour la Recherche Médicale. This work was supported by the CEA, the CNRS and grants from the Association Française contre les Myopathies to M.l.M.

* To whom correspondence should be addressed at SBPM/DBCM/CEA, Bât 528, C. E. de Saclay, 91191 Gif-sur-Yvette, Cedex, France. Phone: (33) 169086243. Fax: (33) 169088139. E-mail: lemairem@dsvidf.cea.fr.

‡ Section de Biophysique des Protéines et des Membranes.

§ Section de Bioénergétique.

|| Danish Biomembrane Research Centre.

⊥ Present address: Laboratoire de Biophysique Moléculaire et Cellulaire, Département de Biologie Cellulaire et Moléculaire, CEA et CNRS Unité de Recherche Associée 520, CEA Grenoble, 38054 Grenoble, Cedex, France.

[1] CD, circular dichroism; COSY, homonuclear correlated spectroscopy; DM, *n*-dodecyl β-D-maltoside; DPC, d_{38}-dodecylphosphocholine; DSS, 2.2-dimethyl-2-silapentane-5-sulfonate; EDTA, ethylenediaminetetraacetic acid; FTIR, Fourier transform infrared spectroscopy; HMQC, ^1H-detected heteronuclear multiple quantum coherence spectroscopy; JR, "jump and return" pulse sequence; NMR, nuclear magnetic resonance; NOE, nuclear Overhauser effect; NOESY, nuclear Overhauser enhancement spectroscopy; PK, proteinase K; SDS, sodium dodecyl sulfate; SERCA, sarco(endo)plasmic reticulum Ca^{2+}-ATPase; SR, sarcoplasmic reticulum; TFE, trifluoroethanol; TM, transmembrane; TOCSY, total correlated spectroscopy.

10.1021/bi983039d CCC: $18.00
Published on Web 04/15/1999

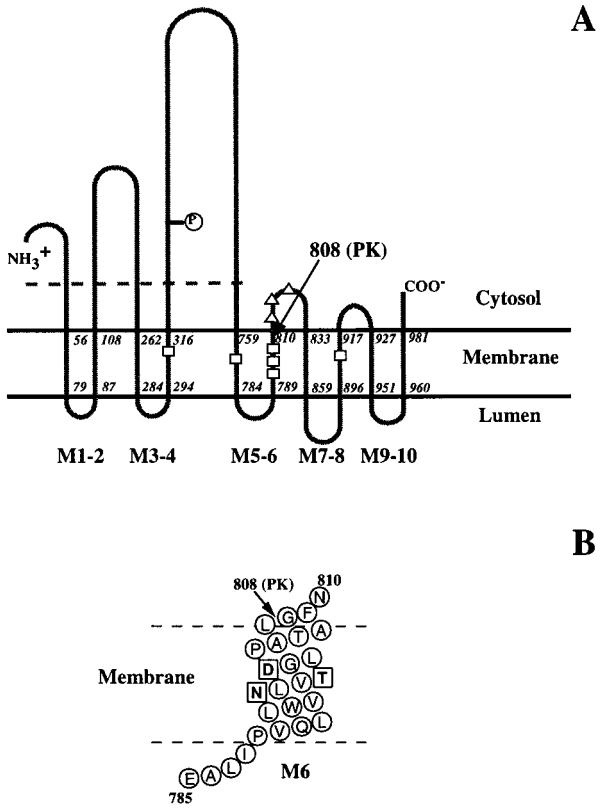

FIGURE 1: Topological model of Ca^{2+}-ATPase and structure prediction of M6 TM segment. (A) Representation of Ca^{2+}-ATPase folding based on the 10 spans model (*12*). Italic numbers refer to the residues predicted to be at the membrane/water interface (*72*). The dashed horizontal line is considered to indicate the top of the stalk. The arrow indicates one of the proteinase K (PK) cleavage sites (*35*, *38*). Circled P indicates the phosphorylable residue Asp 351. Open boxes in the membrane part correspond to critical residues for Ca^{2+}-binding: Glu 309, Glu 771, Asn 796, Thr 799, Asp 800, and Glu 908 (*32*). Open triangles in the cytoplasmic loop L6/7 correspond to critical residues for initial steps in Ca^{2+}-binding: Asp 813, Asp 815, Asp 818 (*35*, *36*). (B) A focus on the transmembrane span M6. The membrane boundary is tentative and takes into account the prediction of (*72*) and the proteinase K cleavage site, at respectively the N-terminus and C-terminus of M6. Bold residues in open boxes are involved in calcium binding (*32*).

ments. From these electron microscopy data as well as from comparison of sequences and other experimental data, Zhang and co-workers (*15*) have proposed a structural model for the organization of the TM segments of Ca^{2+}-ATPase in the membrane, which however still needs to be confirmed.

In addition to crystallographic studies, NMR spectroscopy can provide conformational information at the residue level on membrane proteins (e.g., refs *16*−*18*, and references therein) or on isolated fragments, especially TM segments incorporated in membrane environment or in organic solvents (e.g., refs *19*−*22*, and references therein). Furthermore, Shon et al. showed that the conformation of the bacteriophage Pf1 coat protein with a single TM segment is very similar in detergent micelle and phospholipid bilayer using solution and solid-state NMR spectroscopies, respectively (*23*). In regard to multispan membrane proteins, such an approach has been exemplified by the work of Arseniev and colleagues (e.g., refs *24*−*26*) performed on peptides corresponding to four TM spans of bacteriorhodopsin. These authors have shown by NMR experiments that the structure of isolated TM spans in the presence of organic solvents or detergent micelles is quite consistent with the structure of the corresponding regions in the whole protein determined by crystallography (*27*). In addition to the determination of secondary structure elements, high-resolution NMR spectroscopy allows the investigation of their conformational flexibility as well as the detection of particular local conformations such as capping motifs (*28*).

We plan to investigate the structure of several of the TM segments of Ca^{2+}-ATPase. As a first step, we focus here on segment M6, which is particularly interesting both from the functional and the structural point of view. Together with M4, M5, and probably M8, the M6 segment is very conserved among SERCA ATPases (*1*) and contributes to the membranous calcium-binding sites. Equilibrium binding isotherms demonstrate that two calcium ions are bound cooperatively and with high affinity (*29*−*31*). Site-directed mutagenesis studies have led to the conclusion that M6 supplies three out of six membranous residues critically involved in calcium binding (*32*, *33*): E309 (M4), E771 (M5), N796/T799/D800 (M6), and E908 (M8) (Figure 1A). All of these residues (except E908) have been found to be essential for occlusion of calcium in the presence of Cr-ATP (*34*). M6 is also very close to the L6/7 loop which probably is involved in the initial interaction of Ca^{2+}-ATPase with calcium on the cytoplasmic side (*35*, *36*). Molecular modeling is consistent with the central role of M6 in the binding of both calcium ions (*37*). From a structural point of view, the M6 region in Ca^{2+}-ATPase and other P-type ATPases presents a number of striking features which suggest deviations from a classical α-helical membrane traverse: while hydropathy plots of the M6 region predict the C-terminal boundary to be at N810 (*12*), proteolysis studies with proteinase K show the presence of a proteolytic site between L807−G808 (ref *38* and Figure 1). In addition, the M5/M6 regions of the Na^+,K^+- and H^+,K^+-ATPases seem to have a flexible topology (ref *39*, and for an illustration, see Figure 7 in ref *1*): for Na^+,K^+-ATPase, it has been shown that, after removal of the ATPase cytoplasmic part by tryptic digestion, the M5/M6 region can be extracted from the membrane, without detergent (*40*); a similar observation has been described for the H^+,K^+-ATPase (*41*). Although the M5/M6 region of Ca^{2+}-ATPase remained associated with the membrane after trypsinolysis (*42*), in vitro translation experiments showed that the isolated TM6 of rat SR Ca^{2+}-ATPase is the only one TM peptide that acted neither as a signal anchor nor a stop transfer signal (*43*) which can be taken as an evidence of a particular structure for this TM. In a previous report, we have observed that the segment M6 of Ca^{2+}-ATPase remains soluble in the absence of detergent in a random coil structure (*44*). However, in the presence of a nonionic detergent (dodecylmaltoside), the M6 peptide exhibits some secondary structure, with Trp794 being embedded within the hydrophobic core of the detergent micelle (*44*).

In this report, we have investigated by NMR the conformational properties of the isolated segment M6, in the presence of DPC micelles, widely used to mimic membrane-like environments. The M6 peptide has been obtained by chemical synthesis and corresponds to the sequence E785−N810 of the Ca^{2+}-ATPase (Figure 1B). This sequence comprises the predicted M6 membrane spanning segment L787−F809, with an additional two residues of the preceding

L5/6 loop and one residue of the following L6/7 loop (*1*). The use of DPC in such experiments has been validated by the pioneering work of Wüthrich's group (*45*). In the present paper, we report the structure of the isolated M6 segment and the effect of TFE and/or calcium addition on its conformation. On the basis of our results, we propose a working model for the conformation and the insertion of the M6 peptide in the membrane.

EXPERIMENTAL PROCEDURES

Peptide Synthesis. The peptide M6 was purchased from K. J. Ross-Petersen, A. S., Chemical Research and Development Laboratory (Denmark). The synthesis was performed using *N*-t-Boc chemistry. To facilitate the assignment of NMR resonances, the following residues were ^{15}N-labeled: L787, V790, L792, V798, G801, A804, and G808. ^{15}N-AA were purchased from EurisoTop, France. The N-terminus was acetylated, and the C-terminus was blocked by an amide group. The purity of the peptide was assessed by ESI/MS and appeared to be more than 95%. For CD measurements, we have used a stock solution of peptide M6 prepared without ^{15}N-labeling, at 2 mg/mL in 20 mM Tris-HCl, pH 7.4.

Circular Dichroism Measurements. Circular dichroism (CD) spectra were recorded on a Jobin Yvon CD6 spectrodichrograph, using 0.5 mm quartz cuvettes at 20 °C. The spectral bandwidth was 2 nm, the wavelength increment and the accumulation time were 1 nm and 2 s/step, respectively. Each spectrum resulted from averaging 10 successive individual spectra. Background spectra of the corresponding buffer were recorded under identical conditions and subtracted. Estimation of α-helical content was done according to ref *46*.

NMR Experiments in DPC Micelles. The sample without TFE was prepared from 4.2 mg of pure peptide (3 mM final), solubilized in 500 μL of 90:10 H_2O/D_2O, 20 mM *d*-Tris-HCl buffer containing 29 mg of d_{38}-DPC (150 mM final; EurisoTop, France), 1 mM NaN_3, and 0.2 mM DSS. The pH was adjusted to 7.3 at room temperature. The sample with TFE was prepared in the same conditions as above, but in addition contained 0.1 mM *d*-EDTA and 20% deuterated d_3-TFE (EurisoTop, France). The pH was adjusted to 7.1. The use of DPC and high pH values (∼7) were required for analyzing the calcium effect in a second step. Sets of TOCSY and NOESY phase-sensitive spectra were collected on Bruker DRX 600 spectrometer at 35 °C. Chemical shifts were referenced from the DSS signal. The water resonance was suppressed either by presaturation or by using the JR sequence (*47*). Respectively, for the samples with 0 or 20% TFE, a total of 64 (TOCSY and NOESY) or 160 (TOCSY) and 80 (NOESY) transients were acquired with a recycling delay of 1 s. Sine-bell functions were used for apodization. The mixing times were 80 and 100 ms for the TOCSY and NOESY experiments, respectively. ^{15}N heteronuclear HMQC-COSY spectra were recorded at 35 °C (*48*). A GARP ^{15}N-decoupling sequence was used in all the experiments. Data were processed using XWINMR software (Bruker). Hα chemical shift indexes were determined using random coil values of ref *49* and those of ref *50* for residues followed by a proline. ^{31}P and ^{2}H NMR spectra were recorded on a Bruker DRX 300 at 121 and 46 MHz, respectively.

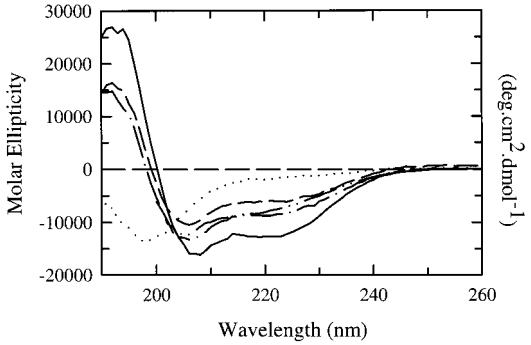

FIGURE 2: Circular dichroism spectra of peptide M6 in the presence of DPC micelles without or with TFE. Dotted line represents M6 in 20 mM Tris-HCl at pH 7.4. Dashed line represents M6 in 20 mM Tris-HCl at pH 7.4, containing in addition 5 mM DPC. Dash−dot and continuous lines represent M6 in the same buffer containing 5 mM DPC, but with 10 or 20% TFE, respectively. Peptide concentration was 30 μM and cell path was 0.5 mm. Temperature was 20 °C. In each case the corresponding buffer background has been subtracted from the spectra shown. Dash−dot−dot line represents the CD spectrum previously obtained for ∼4 μM M6 in the presence of 4 mM DM (for more details see legend of Figure 8 in ref *44*).

NMR Experiments in SDS Micelles. The sample without TFE was prepared from 5.2 mg of pure peptide (3 mM final), solubilized in 600 μL of 90:10 H_2O/D_2O, 20 mM *d*-Tris-HCl buffer containing 47.5 mg of d_{25}−SDS (300 mM final; EurisoTop, France), 0.1 mM *d*-EDTA, 1 mM NaN_3, and 0.2 mM DSS. The sample with TFE was prepared in the same conditions as above, but in addition contained 20% deuterated d_3-TFE (EurisoTop, France). In both conditions, the pH was adjusted to 3. For exchange experiments, samples were solubilized in pure D_2O solution after lyophilization. NMR spectra were recorded on Bruker DRX 500 spectrometer. Respectively, for the samples with 0 or 20% TFE, a total of 64 or 32 (TOCSY and NOESY) transients were acquired, with a recycling delay of 1 s. The mixing times were 80 ms for the TOCSY and 120 ms for the NOESY experiments. Other conditions are similar to those for DPC micelles.

FTIR. The FTIR sample consisted of ∼10 μL of the buffer or peptide solution (the conditions are similar to those for NMR samples) deposited between two calcium fluoride windows. FTIR spectra were recorded using a Bruker IFS 88 SX spectrometer equipped with a MCT detector and a N_2-cooled cryostat (Oxford-instrument). All spectra were recorded at 17 °C at a resolution of 4 cm^{-1}. For each spectrum, 512 scans were summed. Spectra obtained with two different samples were averaged. Buffer subtraction was carried out digitally to give a straight baseline in the region 2500−1800 cm^{-1}.

RESULTS

Circular Dichroism Data. CD spectra of the M6 peptide were recorded in the absence or presence of detergent micelles. As previously mentioned, M6 was found to be easily soluble even in the absence of detergent (*44*). The CD spectrum shows that under these conditions the conformation of M6 corresponds to a random coil state (Figure 2, dotted line). In the presence of DPC micelles, the CD spectrum of M6 exhibits a much larger negative molar ellipticity in the 205−240 nm range, indicative of the formation of secondary structures (Figure 2, dashed line).

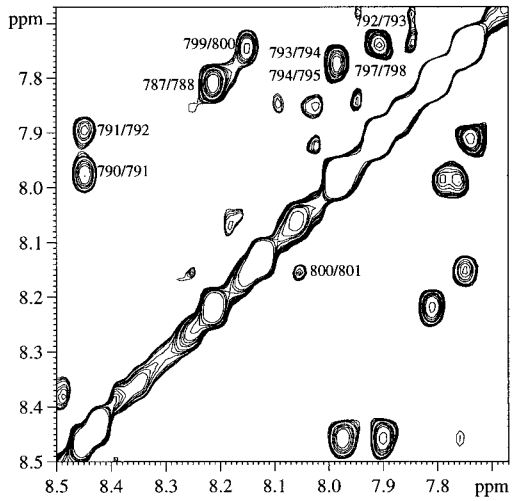

FIGURE 3: Amide proton region of the NOESY spectrum (500 MHz, mixing time 120 ms) for the peptide M6 solubilized in DPC micelles at 35 °C and pH 7.3, without TFE.

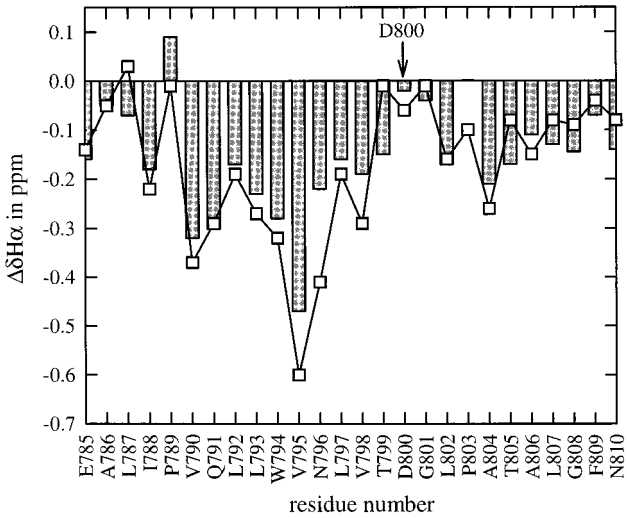

FIGURE 4: α-Proton chemical shift indexes, $\Delta\delta H\alpha = \delta H\alpha_{obs} - \delta H\alpha_{coil}$, for peptide M6 solubilized in DPC micelles in absence (grey bars) or in the presence of 20% TFE (white squares; continuous line) at 35 °C and pH 7.3 or 7.1, respectively. For each Gly residue, the mean $\Delta\delta H\alpha$ is indicated.

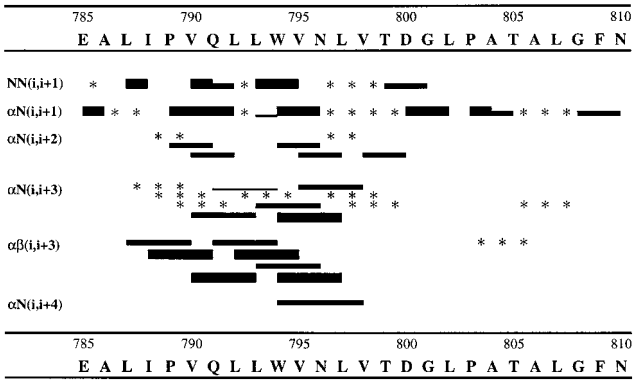

FIGURE 5: NOE connectivities in peptide M6 in the presence of DPC micelles at pH 7.3 and 35 °C, without TFE. The width of αN, NN, etc., corresponds to the intensity of the NOE cross-peaks measured from the two-dimensional NOESY experiment. Stars represent ambiguous NOE connectivities probably present but hidden by other peaks.

The CD signal at 222 nm suggests about 25% of α-helix conformation. A similar helix content was observed using another detergent, the nonionic *n*-dodecyl β-D-maltoside (*44*): for the sake of comparison, the previously obtained CD spectrum in the presence of DM (*44*) is also reported in the Figure 2 (dash−dot−dot line). In the presence of DPC micelles, addition of 10 or 20% TFE (v/v), well-known for stabilizing helix structures, results in an increase of the molar ellipticity of the CD signal (Figure 2). After addition of 20% TFE, the α-helix content reaches a value of about 42%. Concentrations of TFE higher than 20% were not used, since above this percentage, a significant effect on micelle structure has been demonstrated (*51*).

NMR data of M6 in DPC micelles without TFE. TOCSY, NOESY, and ^{15}N-HMQC-COSY experiments of selectively ^{15}N-labeled M6 solubilized in the presence of deuterated-DPC were performed. The amide proton region of a M6 NOESY spectrum is shown in Figure 3. Sets of NMR experiments were recorded in the absence or in the presence of 20% TFE at pH ~7.2. In both conditions, full assignment of M6 proton resonances was achieved (see Supporting Information). Figure 4 shows the Hα chemical shift index value ($\Delta\delta H\alpha$) for each residue of M6 solubilized in DPC micelles either in the absence (grey bars) or presence of 20% TFE (white squares). The $\Delta\delta H\alpha$ values of I788 and L802 were corrected to account for the effect of the adjacent proline residues (*50*).

As shown in Figure 4, in the absence of TFE (see below the description of the TFE effect), large negative chemical shift indexes are observed between I788 and T799, indicating that this segment adopts a predominantly helical structure. The intense V795 $\Delta\delta H\alpha$ value most probably results from ring current effects due to W794. The $\Delta\delta H\alpha$ profile shows that the following G801−N810 segment is less structured, but with indexes predominantly still negative.

In agreement with the Hα data, the network of NOE correlations (Figure 5) is consistent with a predominantly helical structure. A number of $\alpha N(i,i+3)$ and $\alpha\beta(i,i+3)$ NOEs are observed in the L787−D800 segment, but only one $\alpha N(i,i+4)$ contact is detected. On the other hand, a number of $\alpha N(i,i+2)$ contacts are observed in this region. These data indicate that the helix is not fully stabilized but undergoes a rapid interconversion between 3_{10} and α conformations. The lack of $NN(i,i+1)$ contacts in the G801−N810 segment shows that this region is rather disordered. Nevertheless possible $(i,i+3)$ contacts can be found in the P803−G808 segment. These contacts may reflect the presence of transient helix turns in agreement with the weak but mainly negative $\Delta\delta H\alpha$ values observed in this segment. Last, the observation of Nδ NOE connectivities between I788 and P789, and between L802 and P803 shows that both prolines are in a predominant trans conformation.

A Schellman Motif Probably Caps the M6 Helix. Referring to our present knowledge on local conformations that lock helix N- and C-termini (for a review, see *28*), it is of interest to observe that the L797VTDGL802 sequence found at the end of the M6 helix satisfies the amino acid distribution characteristic of a C-cap Schellman motif, i.e., hxpxGh where x can be any residue, h are hydrophobic residues, p is a polar residue, and G is a glycine residue (G801 in M6). Following the helix residue numbering of ref *52*, the hxpxGh sequence can be written as C3C2C1CcC′C″ where Cc (D800) is the C-cap residue. In NMR spectra, the Schellman motif is usually characterized by side-chain to side-chain $(i,i+5)$

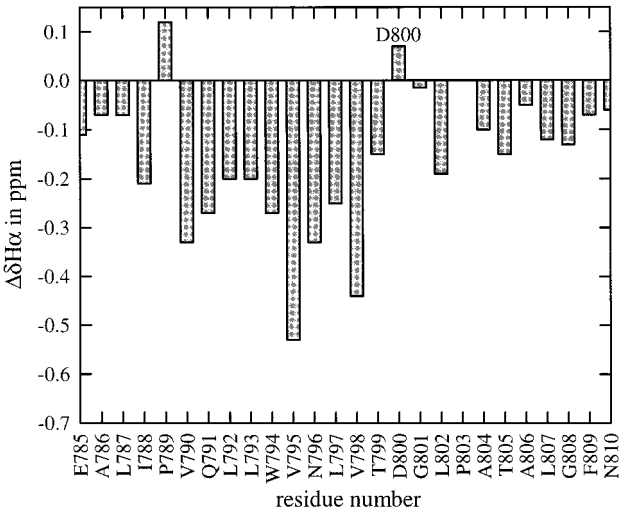

FIGURE 6: α-Proton chemical shift indexes, for peptide M6 solubilized in SDS micelles at 35 °C and pH 3. For each Gly residue, the mean ΔδHα is indicated.

FIGURE 7: NOE connectivities in peptide M6 in the presence of DPC micelles and 20% TFE at pH 7.1 and 35 °C. The width of αN, NN, etc., corresponds to the intensity of the NOE cross-peaks measured from the two-dimensional NOESY experiment. Stars represent ambiguous NOE connectivities probably present but hidden by other peaks.

NOEs between the two hydrophobic residues at positions C3 and C″ (53). This motif is also characterized by the formation of two hydrogen bonds between C″ → C3 and C′ → C2 (*54*). In the case of M6, it was not possible to unambiguously assign such *i*,*i*+5 NOEs because of numerous signal overlaps in the concerned spectral region. Indeed, both C3 and C¢¢ residues of the Schellman motif in M6 are leucines (L797, L802) which are present together with four other Leu residues in the peptide. But, the fact that the helical structure stops at the level of residue D800 strengthens the hypothesis that the Schellman motif in the M6 sequence is actually formed at least transiently.

H/D Exchange Rate and Insertion of M6 in the Micelles. It was of interest to conduct NMR experiments at low pH (i) to investigate the effect of the D800 protonation on the insertion of M6 in the detergent micelles and (ii) to observe the H/D exchange rates of the amide groups. Unfortunately, at low pH in the presence of DPC micelles, M6 precipitates. We have therefore solubilized M6 in the presence of anionic deuterated-SDS micelles, also frequently used for studying membrane peptide by high-resolution NMR (e.g., refs *26* and *55*). In the presence of SDS and at pH 3, M6 does not precipitate, and furthermore, the corresponding ΔδHα profile pattern was found quite close to that observed in DPC micelles (Figure 6). These results indicate that the conformation and the insertion of the M6 peptide are not affected by the different micellar environments as well as by the D800 protonation. H/D exchange experiments show that only the amide protons in the I788−V798 segment (except for N796) are slowly exchangeable, i.e., are still observed after several hours, while the H/D exchange for the remaining residues (except for L807) is observed within minutes (data not shown). Note that we cannot detect the amide protons of G801 and L802 in D_2O, which are the two residues involved in the hydrogen bonds characterizing the Schellman motif (between L802 → L797 and G801 → V798). The H/D exchange experiments suggest that the N-terminal I788−V798 segment is embedded in the hydrophobic environment of the micelles, whereas the C-terminal segment is exposed at the micellar interface and/or in the aqueous solution.

Effect of TFE. After addition of 20% TFE in the presence of DPC micelles, the overall ΔδHα profile pattern is conserved (Figure 4, white squares). The main effect of TFE is to increase the ΔδHα indexes in the I788−V798 segment. The corresponding NOE network (Figure 7) confirms the stabilization of this region as an α-helical structure since a continuous set of (*i*,*i*+4) contacts are detected, whereas only one (*i*,*i*+2) NOE remains present. Furthermore, addition of TFE allowed us to detect in the G801−L807 region (Figure 7) several (*i*,*i*+3) NOEs and one (*i*,*i*+4) NOE, not observed in a pure micellar environment. These NOEs confirm the helical propensity of the C-terminal segment G801−L807 revealed by the negative ΔδHα indexes. It has to be pointed out that the two helical segments detected in the presence of TFE are linked by a region containing the critical residues T799 and D800, involved in the Ca^{2+} binding in the entire Ca^{2+}-ATPase (*32*). In SDS micelles and after addition of 20% TFE, the amide H/D exchange rates in the C-terminal segment (data not shown) are as fast as in the absence of TFE, indicating that this region remains exposed to the aqueous solution.

Effect of Calcium Ions. In the absence of TFE, the NMR spectrum of M6 in DPC micelles is not affected upon addition of calcium up to 30 mM (data not shown). In the presence of 20% TFE, addition of increasing calcium concentrations up to 2 mM has no effect on the M6 spectrum. However, at 3 mM Ca^{2+} (i.e., by addition of 1 mol of calcium/mol of M6), we observed that the high-resolution NMR spectrum of M6 is suddenly lost with only 10% of the initial resonance intensity still remaining (data not shown). Visual inspection of the sample showed that under these conditions the solution remains transparent. However, the apparent viscosity is dramatically increased, suggesting the formation of a gel. We found that this phase transition was not reversed after addition of 4 mM EDTA and a temperature increase up to 80 °C for a few minutes.

Using the same experimental conditions as above, another set of ^1H NMR experiments was performed on a new sample and completed by recording ^{31}P and ^2H NMR spectra. The two latter spectra allowed us to follow the evolution of the signals of DPC (phosphorus and deuterons) as well as those of the TFE and Tris (deuterons). At 3 mM Ca^{2+}, the loss of the high-resolution ^1H NMR spectrum occurred as before, but neither the ^{31}P nor the ^2H NMR spectra were perturbed (data not shown). In a parallel experiment performed under

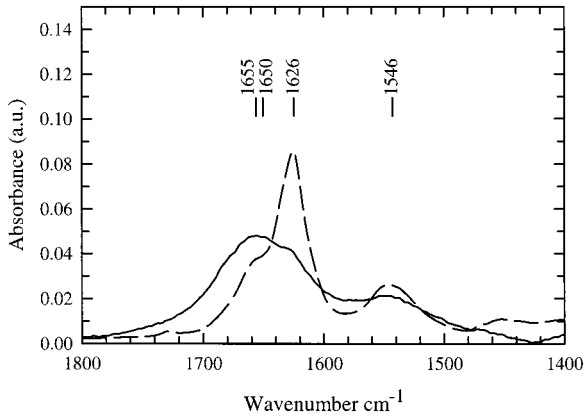

FIGURE 8: FTIR spectra of M6 peptide in the presence of d-DPC micelles, 20% TFE and 10% D_2O at pH 7.1, before (continuous line) or after (dashed line) addition of 1 mol of calcium/mol of protein.

```
PHDsec              EEHHHHHHHH     HHHH
M6      785 EALIPVQLLWVNLVTDGLPATALGFN 810
                    |  |  |||||
M4      293 YYFKIAVALAVAAIPEGLPAVITTCL 319
PHDsec  HHHHHHHHHHHHHHHH     HHHHHH
```

FIGURE 9: Amino acid sequences of M6 in comparison with M4, and their secondary structure prediction by PHDsec (*73*, *74*). The alignment of the two sequences was made from the D/EGL region (*64*). The letters indicate the secondary structure type: H for helix, E for extended (sheet), blank for others (e.g., loop conformations). Continuous and dotted vertical lines indicate respectively identical or similar residues in both sequences. Bold residues in open boxes are involved in calcium binding (*32*).

the same conditions but in the absence of peptide, no gel formation occurred. These data indicate that the "gel" structure results from a self-association of M6 monomers upon calcium binding, while the DPC micelles are unaffected.

The effect of calcium on the secondary structure of the M6 peptide in the gel phase has also been analyzed by FTIR spectroscopy (Figure 8). The spectrum recorded in the absence of calcium, but in the presence of 20% TFE (continuous line), it shows an absorption maximum at 1655 cm^{-1} indicative of the presence of helical structure in agreement with the CD and NMR data. However other weak components are observed such as a β-sheet structure (at 1626 cm^{-1}) probably reflecting aggregated peptides, since this form was not detected in high-resolution NMR spectra. In the presence of 3 mM calcium, the FTIR spectrum (dotted line) clearly shows that the helical structure disappears at the expense of β-sheet structure.

DISCUSSION

In general, topological models of Ca^{2+}-ATPase predict that the M6 TM span is in a helical conformation covering approximately 20−25 residues. However, prediction using the PHD algorithm (Figure 9) as well as previous studies from Andersen and Vilsen (*4*, *56*) suggested that M6 may not behave as a classical TM α-helix. From functional data on calcium binding, these authors suggest the possible existence of a disorganized structure of the M5/M6 region, similar to a mobile loop or "short inner helices" in addition to β-structure (*57*). In this context, it is of interest that our NMR data obtained on the isolated M6 peptide, are consistent

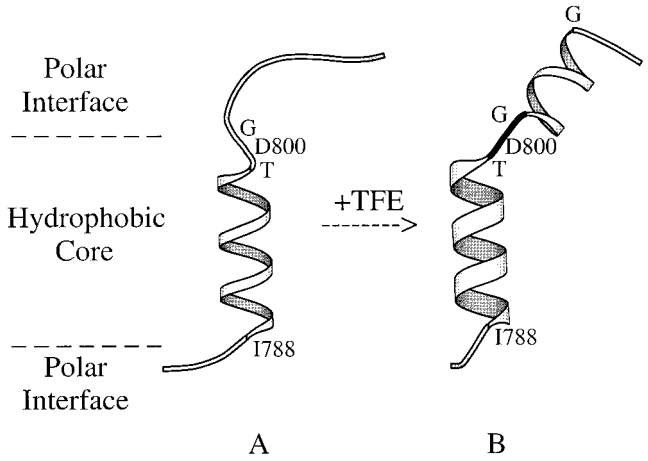

FIGURE 10: Working model of M6 in membranes, designed using the MolScript software (*75*). The peptide M6 is represented in the absence (A) or in the presence of TFE (B). The ribbons correspond to the I788-T799 helix in panels A and B and to the G801-G808 helix in panel B. The ribbon thickness is representative of the structure stability. The black region corresponds to the T799-G801 segment.

with a conformation comprising a short 12 residue-helix I788−T799 buried in the hydrophobic core and a less structured C-terminal segment G801−N810 located in the interfacial and/or the aqueous environment. However, in the presence of TFE, characterized by a low dielectric constant (*58*) close to that of a membrane/water interface (*59*), the C-terminal part tends to adopt a helical conformation, with a remaining flexible "hinge" region comprising T799 and D800, i.e., two of the critical calcium-binding residues. A working model summarizing the conformational properties of M6 is displayed in Figure 10. In agreement with our finding that the N-terminal helix ends near the critical residues T799 and D800, we showed that they are included in the $L_{797}VTDGL_{802}$ sequence corresponding to a Schellman motif, a well-known stop signal for the C-terminal propagation of α-helices, inducing a bend of the backbone with respect to the helix axis. The capping motifs have been essentially investigated in the case of water-soluble proteins (*28*). However, from examination of the available crystallographic data, such motifs are also present in membrane proteins. For example, in the 3D structure of the photosynthetic reaction center of *Rhodopseudomonas viridis* (*60*), formation of Schellman motifs can be observed at the extremities of several TM helices in subunits M and L (*61*). Note that, in some cases, Schellman motifs are formed although the related sequences do not fully correspond to the canonical amino acid distribution given by Aurora et al. (*62*).

Interestingly, mutation of G801, a key residue of the putatif C-cap motif in M6, to the much more bulky residue valine has dramatic effects on the enzyme function since it abolishes calcium transport activity (*63*). A glycine residue is also present in the transmembrane segments M4 and M5 both assumed to participate with M6 (and probably M8) in the calcium-binding sites. This residue is the central part of the consensus sequence (D/E)G(L/V) shared by M4, M5 (reversed sequence), and M6 first noted by Rice et al. (*64*). Although in M4 and M5 the sequences do not fulfill the exact requirements for a Schellman motif, this does not exclude its formation as noted above (*61*).

Within the native ATPase, there are two direct lines of evidence in favor of the C-terminal accessibility of M6. First, a proteolytic site (*35*, *38*) has been found at the end of M6, between L807 and G808, before the predicted membrane/water interface, despite that it is generally considered that proteolytic sites are localized in a flexible loop at least 4−8 residues above the membrane interface (*1*). Second, competitive Elisa experiments carried out with the p796−807 antibody directed toward the M6 segment have shown that the 796−807 epitope is exposed at the membrane/cytosol interface in particular after PK treatment or $C_{12}E_8$ solubilization of the SR Ca^{2+}-ATPase (*65*).

In native Ca^{2+}-ATPase, it has been suggested that M6 together with M4 may adopt a unique helix conformation comprising about 20 residues. This was inferred from site-directed disulfide mapping (*66*), which indicates that, in the intact structure, M4 and M6 are in close contact at least under conditions favoring the E2 conformation, with an arrangement predicted to be a right-handed coiled-coil structure. This prediction is based on the observation of cross-links between Cys residues introduced in the C-terminal parts of M4 and M6 (cross-linking efficiency of about 52%, an average of three values: 48, 34, and 74%, respectively, between residues 321/808, 317/807, and 317/804), and toward the N-terminal parts of M4 and M6 (cross-linking efficiency of about 15%, an average of two identical values between residues 305/793 and 305/792). However, much weaker interactions were observed in the intervening region, corresponding to the location of the putative Ca^{2+}-binding sites (cross-linking efficiency of about 3%, an average of four values: 4, ∼4, ∼1, and ∼ 4, respectively between 310/800, 309/796, 309/799, and 309/800). We suggest that the lack of helical structure that we observed in this central region of M6 could indicate the existence of a Ca^{2+}-binding cavity and be the reason for this low cross-linking. Molecular modeling of the clustered M4, M5, M6, and M8 TM segments (*37*) indicates that it is possible to arrange the side chains of relevant residues to yield two discrete and unique areas with valence points analogous to those demonstrated for the duplex calcium-binding sites in the high-resolution structure of other proteins. It is difficult, however, to position favorably the side chains of the three M6 residues (N796, T799, and D800 implied by mutational analysis) simultaneously, due to their diverging orientation if the entire M6 is assumed to be a helix (*37*). A specific advantage derived from our model with a flexible region in M6 is that it allows more freedom and simultaneous participation of N796, T799, and D800 in the complexation of two calcium ions. In the structure of Ca^{2+}-ATPase, obtained from two-dimensional crystals at 8 Å resolution (*15*), the rodlike densities seen within the TM domain are considered to represent helical segments. However, it should be noted that, in this analysis, only nine rodlike densities could be easily fitted, while the tenth one (named I) was observed mainly at the luminal end. Furthermore, in the density cross sections, some helices (C and F) appear weaker in the central part of the membrane, resulting in the formation of a cavity between three TM segments (B, E and F; M6 in their model being B or F) in the middle of the membrane. These features would also be consistent with the presence of a Ca^{2+}-binding cavity in the membrane, corresponding to the location of critical Ca^{2+}-binding residues.

Another aspect of the conformational flexibility characterizing the isolated M6 peptide would be the ability to participate in topological rearrangements relevant for Ca^{2+}-ATPase transport. It is generally agreed that, during the functional cycle, Ca^{2+}-ATPase undergoes significant conformational changes (e.g., refs *67* and *68*). The involvement of M6 in these conformational changes is also supported by a number of experimental findings. First, the proteolytic site located at G808 is less accessible to proteinase K in the presence of high calcium concentrations (*38*). Second, it has been shown that, in Na^+,K^+-ATPase from which the cytosolic regions have been removed by tryptic treatment, the M5/M6 segment is easily extractable from the membranes in the absence of occluding cation (*40*). Third, in the case of the H^+,K^+-ATPase, the residue C822 located in the sixth TM segment and homologous to V798 in the Ca^{2+}-ATPase is accessible to omeprazole, a probe of extracytoplasmic thiols (*39*). Plasticity has also been suggested for the neighboring M7/M8 segment in the Ca^{2+}-ATPase (*13*). From these observations, it appears that the topology of the M5/M6 region possesses an intrinsic flexibility that could be required for ATPase function. The presence of a hinge region in M6 would therefore be consistent with the view that the Ca^{2+}-ATPase functional cycle involves switches between several conformations.

We observed that addition of high concentrations of calcium to M6 in DPC micelles and in the presence of TFE, gave rise to irreversible self-association of the peptide, leading to a gel formation. This observation may result from the formation of nonspecific salt bridges between M6 monomers involving the three residues (N796, T799, and D800) known to participate in the calcium binding but would perhaps also involve Q791 and T805. As observed by FTIR, the self-association leads to the formation of nonnative β-sheet structures. These results also show that in the absence of specific long-range tertiary interactions (provided essentially by M4 and M5 in our case), isolated fragments of membrane proteins may adopt nonnative structures. This point concerning isolated peptides is illustrated by the recent work of Hunt et al. (*69*, *70*), showing that, among the seven peptides corresponding to each of the seven bacteriorhodopsin helices and reconstituted in phospholipid vesicles, five fragments (A−E) adopt a helical conformation whereas one fragment (F) is fully disordered and another (G) forms a nonnative β-sheet structure. Note however, that Barsukov et al. (*24*) have shown by NMR in organic solution that the isolated proteolytic fragment corresponding to the transmembrane regions F and G forms two helices with amino acid boundaries very similar to the ones observed in the 3D-crystallographic structure (*27*).

Concluding Comments. In further studies, it will be of interest to investigate the conformational properties of other isolated peptides corresponding to the M4 or M5 spans and to investigate their interactions with M6 in the presence of calcium ions. According to the results reported in the present paper, one may expect to obtain a description at the residue level of the M4−M5−M6 cluster in a membrane-like environment. Whatever the outcome of such interactions, which are likely to be technically difficult but feasible (*71*), the present study indicates that the central part of M6 involved in the Ca^{2+} binding has no tendency to be helical. In addition, its C-terminal part is not included in a nonpolar

environment and therefore is not likely to be surrounded by lipids, a fact which is also supported by sequence comparison (*15*). Remarkably, the PHD prediction algorithm of secondary structure suggests that each of both M6 and M4 peptides forms two distinct helical segments separated by the D/EGL motif (Figure 9). This is not the case for the other predicted TM segments. All these considerations, including our data and the fact that M4 and M6 are the most highly conserved TM segment among SERCA ATPases (*1*), point out that the C-terminal parts of M6 and M4, together with the N-terminal part of M5, could constitute the mouth of a pore, providing access to the Ca^{2+}-binding sites.

ACKNOWLEDGMENT

We thank Dr. A. Sanson for many stimulating discussions and his help in preparing Figure 10, Drs. F. Penin, F. Cordier, P. Falson, Ch. Jaxel, B. de Foresta, Ph. Champeil and the referees for helpful suggestions.

SUPPORTING INFORMATION AVAILABLE

^1H chemical shifts of peptide M6 solubilized in DPC micelles with 0 or 20% TFE. This material is available free of charge via the Internet at http://pubs.acs.org.

REFERENCES

1. Møller, J. V., Juul, B., and le Maire, M. (1996) *Biochim. Biophys. Acta 1286*, 1−51.
2. Makinose, M. (1973) *FEBS Lett. 37*, 140−143.
3. de Meis, L., and Vianna, A. L. (1979) *Annu. Rev. Biochem. 48*, 275−292.
4. Andersen, J. P., and Vilsen, B. (1995) *FEBS Lett. 359*, 101−106.
5. Andersen, J. P. (1995) *Biosci. Rep. 15*, 243−261.
6. Inesi, G., Chen, L., Sumbilla, C., Lewis, D., and Kirtley, M. E. (1995) *Biosci. Rep. 15*, 327−339.
7. Champeil, P. (1996) in *Biomembranes* (Lee, A. G., Ed.) vol. 5, pp 43−76, JAI press Inc., Greenwich, CT.
8. Martonosi, A. N. (1996) *Biochim. Biophys. Acta 1275*, 111−117.
9. Mintz, E., and Guillain, F. (1997) *Biochim. Biophys. Acta Bioenerget. 1318*, 52−70.
10. MacLennan, D. H., Rice, W. J., and Green, N. M. (1997) *J. Biol. Chem. 272*, 28815−28818.
11. Meissner, G. (1994) *Annu. Rev. Physiol. 56*, 485−508.
12. Brandl, C. J., Green, N. M., Korczak, B., and MacLennan, D. H. (1986) *Cell 44*, 597−607.
13. Møller, J. V., Ning, G., Maunsbach, A. B., Fujimoto, K., Asai, K., Juul, B., Lee, Y.-J., Gomez de Gracia, A., Falson, P., and le Maire, M. (1997) *J. Biol. Chem. 272*, 29015−29032.
14. Auer, M., Scarborough, G. A., and Kühlbrandt, W. (1998) *Nature 392*, 840−843.
15. Zhang, P., Toyoshima, C., Yonekura, K., Green, N. M., and Stokes, D. L. (1998) *Nature 392*, 835−839.
16. Marassi, F. M., and Opella, S. J. (1998) *Curr. Opin. Struct. Biol. 8*, 640−648.
17. Papavoine, C. H., Christiaans, B. E., Folmer, R. H., Konings, R. N., and Hilbers, C. W. (1998) *J. Mol. Biol. 282*, 401−419.
18. Weers, P. M., Wang, J., Van der Horst, D. J., Kay, C. M., Sykes, B. D., and Ryan, R. O. (1998) *Biochim. Biophys. Acta 1393*, 99−107.
19. Morein, S., Trouard, T. P., Hauksson, J. B., Rilfors, L., Arvidson, G., and Lindblom, G. (1996) *Eur. J. Biochem. 241*, 489−497.
20. Doak, D. G., Mulvey, D., Kawaguchi, K., Villalain, J., and Campbell, I. D. (1996) *J. Mol. Biol. 258*, 672−687.
21. Pellegrini, M., Bisello, A., Rosenblatt, M., Chorev, M., and Mierke, D. F. (1998) *Biochemistry 37*, 12737−12743.
22. Lambotte, S., Jasperse, P., and Bechinger, B (1998) *Biochemistry 37*, 16−22.
23. Shon, K. J., Kim, Y., Colnago, L. A., and Opella, S. J. (1991) *Science 252*, 1303−1305.
24. Barsukov, I. L., Abdulaeva, G. V., Arseniev, A. S., and Bystrov, V. F. (1990) *Eur. J. Biochem. 192*, 321−327.
25. Lomize, A. L., Pervushin, K. V., and Arseniev, A. S. (1992) *J. Biomol. NMR 2*, 361−372.
26. Pervushin, K. V., and Arseniev, A. S. (1992) *FEBS Lett. 308*, 190−196.
27. Pebay-Peyroula, E., Rummel, G., Rosenbusch, J. P., and Landau, E. M. (1997) *Science 277*, 1676−1681.
28. Aurora, R., and Rose, G. D. (1998) *Protein Sci. 7*, 21−38.
29. Inesi, G., Kurzmack, M., Coan, C., and Lewis, D. E. (1980) *J. Biol. Chem. 255*, 3025−3031.
30. Forge, V., Mintz, E., and Guillain, F. (1993) *J. Biol. Chem. 268*, 10953−10960.
31. Forge, V., Mintz, E., and Guillain, F. (1993) *J. Biol. Chem. 268*, 10961−10968.
32. Clarke, D. M., Loo, T. W., Inesi, G., and MacLennan, D. H. (1989) *Nature 339*, 476−478.
33. Strock, C., Cavagna, M., Peiffer, W. E., Sumbilla, C., Lewis, D., and Inesi, G. (1998) *J. Biol. Chem. 273*, 15104−15109.
34. Vilsen, B., and Andersen, J. P. (1992) *J. Biol. Chem. 267*, 3539−3550.
35. Falson, P., Menguy, T., Corre, F., Bouneau, L., Gomez de Gracia, A., Soulié, S., Centeno, F., Møller, J. V., Champeil, P., and le Maire, M. (1997) *J. Biol. Chem. 272*, 17258−17262.
36. Menguy, T., Corre, F., Bouneau, L., Deschamps, S., Møller, J. V., Champeil, P., le Maire, M., and Falson, P. (1998) *J. Biol. Chem. 273*, 20134−20143.
37. Chen, L., Sumbilla, C., Lewis, D., Zhong, L., Strock, C., Kirtley, M. E., and Inesi, G. (1996) *J. Biol. Chem. 271*, 10745−10752.
38. Juul, B., Turc, H., Durand, M. L., Gomez de Gracia, A., Denoroy, L., Møller, J. V., Champeil, P., and le Maire, M. (1995) *J. Biol. Chem. 270*, 20123−20134.
39. Lambrecht, N., Corbett, Z., Bayle, D., Karlish, S. J., and Sachs, G. (1998) *J. Biol. Chem. 273*, 13719−13728.
40. Lutsenko, S., Anderko, R., and Kaplan, J. H. (1995) *Proc. Natl. Acad. Sci. U S A 92*, 7936−7940.
41. Gatto, C., Lutsenko, S., Shin, J. M., Sachs, G., and Kaplan, J. H. (1999) *Biophys. J. 76*, A450.
42. Shin, J. M., Kajimura, M., Arguello, J. M., Kaplan, J. H., and Sachs, G. (1994) *J. Biol. Chem. 269*, 22533−22537.
43. Bayle, D., Weeks, D., and Sachs, G. (1995) *J. Biol. Chem. 270*, 25678−25684.
44. Soulié, S., de Foresta, B., Møller, J. V., Bloomberg, G. B., Groves, J. D., and le Maire, M. (1998) *Eur. J. Biochem. 257*, 216−227.
45. Lauterwein, J., Bösch, C., Brown, L. R., and Wüthrich, K. (1979) *Biochim. Biophys. Acta 556*, 244−264.
46. Chen, Y.-H., Yang, J. T., and Chau, K. H. (1974) *Biochemistry 13*, 3350−3359.
47. Plateau, P., and Guéron, M. (1982) *J. Am. Chem. Soc. 104*, 7310−7311.
48. Gronenborn, A. M., Bax, A., Wingfield, P. T., and Clore, G. M. (1989) *FEBS Lett. 243*, 93−98.
49. Merutka, G., Dyson, H. J., and Wright, P. E. (1995) *J. Biomol. NMR 5*, 14−24.
50. Wishart, D. S., Bigam, C. G., Holm, A., Hodges, R. S., and Sykes, B. D. (1995) *J. Biomol. NMR 5*, 67−81.
51. Killian, J. A., Trouard, T. P., Greathouse, D. V., Chupin, V., and Lindblom, G. (1994) *FEBS Lett. 348*, 161−165.
52. Harper, E. T., and Rose, G. D. (1993) *Biochemistry 32*, 7605−7609.
53. Viguera, A. R., and Serrano, L. (1995) *J. Mol. Biol. 251*, 150−160.
54. Blanco, F. J., Ortiz, A. R., and Serrano, L. (1997) *Folding Des. 2*, 123−133.
55. Pervushin, K. V., Orekhov, V., Popov, A. I., Musina, L., and Arseniev, A. S. (1994) *Eur. J. Biochem. 219*, 571−583.
56. Andersen, J. P., and Vilsen, B. (1994) *J. Biol. Chem. 269*, 15931−15936.

57. Andersen, J. P., and Vilsen, B. (1998) *Trends Cardiovasc. Med. 8*, 41−48.
58. Llinás, M., and Klein, M. P. (1975) *J. Am. Chem. Soc. 97*, 4731−4737.
59. Wimley, W. C., and White, S. H. (1996) *Nat. Struct. Biol. 3*, 842−848.
60. Deisenhofer, J., Epp, O., Sinning, I., and Michel, H. (1995) *J. Mol. Biol. 246*, 429−457.
61. Duneau, J. P. (1997) Ph.D. Thesis, University of Orléans, France.
62. Aurora, R., Srinivasan, R., and Rose, G. D. (1994) *Science 264*, 1126−1130.
63. Andersen, J. P., Vilsen, B., and MacLennan, D. H. (1992) *J. Biol. Chem. 267*, 2767−2774.
64. Rice, W. J., and MacLennan, D. H. (1996) *J. Biol. Chem. 271*, 31412−31419.
65. Møller, J. V., Juul, B., Lee, Y.-J., le Maire, M., and Champeil, P. (1994) in *The Sodium Pump* (Bamberg, E., and Schoner, W., Eds.) pp 131−134, Springer-Verlag, New York.
66. Rice, W. J., Green, N. M., and MacLennan, D. H. (1997) *J. Biol. Chem. 272*, 31412−31419.
67. Canet, D., Forge, V., Guillain, F., and Mintz, E. (1996) *J. Biol. Chem. 271*, 20566−20572.
68. Ogawa, H., Stokes, D. L., Sasabe, H., and Toyoshima, C. (1998) *Biophys. J. 75*, 41−52.
69. Hunt, J. F., Earnest, T. N., Bousché, O., Kalghatgi, K., Reilly, K., Horváth, C., Rothschild, K. J., and Engelman, D. M. (1997) *Biochemistry 36*, 15156−15176.
70. Hunt, J. F., Rath, P., Rothschild, K. J., and Engelman, D. M. (1997) *Biochemistry 36*, 15177−15192.
71. MacKenzie, K. R., Prestegard, J. H., and Engelman, D. M. (1997) *Science 276*, 131−133.
72. Clarke, D. M., Loo, T. W., and MacLennan, D. H. (1990) *J. Biol. Chem. 265*, 17405−17408.
73. Rost, B., and Sander, C. (1993) *J. Mol. Biol. 232*, 584−599.
74. Rost, B., and Sander, C. (1994) *Proteins 19*, 55−72.
75. Kraulis, P. J. (1991) *J. Appl. Crystallogr. 24*, 946−950.

BI983039D